Received: 24 September 2018 | Revised: 28 January 2019 | Accepted: 30 January 2019

DOI: 10.1002/mrm.27704

FULL PAPER

Magnetic Resonance in Medicine

Analysis of magnetization transfer (MT) influence on quantitative mapping of T_2 relaxation time

Dvir Radunsky[1] | Tamar Blumenfeld-Katzir[1] | Osnat Volovyk[2] | Assaf Tal[2] | Daniel Barazany[3] | Galia Tsarfaty[4] | Noam Ben-Eliezer[1,5,6]

[1]Department of Biomedical Engineering, Tel Aviv University, Tel Aviv, Israel

[2]Department of Chemical Physics, The Weizmann Institute, Rehovot, Israel

[3]Strauss computational neuroimaging center, Tel Aviv University, Tel Aviv, Israel

[4]Department of Diagnostic Imaging, Sheba Medical Center, Ramat Gan, Israel

[5]Sagol School of Neuroscience, Tel Aviv University, Tel Aviv, Israel

[6]Center for Advanced Imaging Innovation and Research (CAI2R), NewYork University Langone Medical Center, New York, New York

Correspondence
Noam Ben-Eliezer, Department of Biomedical Engineering, Tel Aviv University, Tel Aviv 6997801, Israel.
Email: noambe@tauex.tau.ac.il

Funding information
Israel Science Foundation, Grant/Award Number: 2009/17

Purpose: Multi-echo spin-echo (MESE) protocol is the most effective tool for mapping T_2 relaxation in vivo. Still, MESE extensive use of radiofrequency pulses causes magnetization transfer (MT)-related bias of the water signal, instigated by the presence of macromolecules (MMP). Here, we analyze the effects of MT on MESE signal, alongside their impact on quantitative T_2 measurements.

Methods: Study used 3 models: in vitro urea phantom, ex vivo horse brain, and in vivo human brain. MT ratio (MTR) was measured between single-SE and MESE protocols under different scan settings including varying echo train lengths, number of slices, and inter-slice gap. MTR and T_2 values were extracted for each model and protocol.

Results: MT interactions biased MESE signals, and in certain settings, the corresponding T_2 values. T_2 underestimation of up to 4.3% was found versus single-SE values in vitro and up to 13.8% ex vivo, correlating with the MMP content. T_2 bias originated from intra-slice saturation of the MMP, rather than from indirect saturation in multi-slice acquisitions. MT-related signal attenuation was caused by slice crosstalk and/or partial T_1 recovery, whereas smaller contribution was caused by MMP interactions. Inter-slice gap had a similar effect on in vivo MTR (21.2%), in comparison to increasing the number of slices (18.9%).

Conclusions: MT influences MESE protocols either by uniformly attenuating the entire echo train or by cumulatively attenuating the signal along the train. Although both processes depend on scan settings and MMP content, only the latter will cause underestimation of T_2.

KEYWORDS

magnetization transfer (MT), MRI signal models, multi spin-echo, quantitative MRI, T_2 mapping, T_2 relaxation

 © 2019 International Society for Magnetic Resonance in Medicine

15222594, 2019, 1, Downloaded from https://onlinelibrary.wiley.com/doi/10.1002/mrm.27704 by Tel Aviv University, Wiley Online Library on [01/02/2023]. See the Terms and Conditions (https://onlinelibrary.wiley.com/terms-and-conditions) on Wiley Online Library for rules of use; OA articles are governed by the applicable Creative Commons License

1 | INTRODUCTION

The field of quantitative MRI (qMRI) has been gaining increased attention owing to its capacity to optimally use the dynamic range of MRI contrast and provide accurate, stable, and most importantly, reproducible information. Quantitative T_2 (qT_2) relaxation is a clinically valuable parameter, with proven applicability to a wide range of pathologies including stroke, multiple sclerosis, cardiac disease, cancer detection, musculoskeletal diseases, and dysregulated iron content.[1-7]

Biased T_2 assessment can occur for various experimental imperfections such as B_0 and B_1 inhomogeneities, MT interactions, flip-angle errors, water exchange between different compartments, and low SNR.[8-11] Although these imperfections affect any type of acquisition, the mapping of qT_2 in vivo is specifically challenging because of the long scan times associated with full spin-echo (SE) acquisitions (10s of min), and the inherent contamination of fast multi-echo SE (MESE) protocols by stimulated and indirect echoes. These cause MESE signals to strongly deviate from the theoretical exponential model $S(t) = S_0\exp[-t/T_2]$ leading to erroneous T_2 estimations.[12] Several qMRI techniques, which successfully overcome this limitation, have been recently developed. These are typically based on improving the MESE signal models to incorporate the effects of stimulated echoes and of the transmit field (B_1^+) inhomogeneities[13-17] or on avoiding the use of spin-echo-based protocols altogether.[18,19] Further to improving the accuracy of measured T_2, these techniques also aim to produce values that are reproducible across scanners and scan settings through the use of full Bloch simulations of the specific MRI pulse sequence being used for data collection.[20,21]

Another factor that can bias the measurement of T_2 is the transfer of magnetization (MT) between the macromolecular pool (MMP) and the free water pool. The incidental saturation of the MMP and subsequent MT can be instigated by the train of refocusing RF pulses used in MESE protocols[17,22] or by the large number of RF pulses in steady-state sequences.[23,24] MT saturation (MT_{SAT}) effects can then occur because of cross-relaxation or chemical exchange between water molecules and the MMP and are particularly apparent in multi-slice versus single-slice acquisitions, owing to the corresponding increase in the number of RF pulses. Because of its low mobility, the MMP can have a very broad spectral line shape, causing it to be indirectly excited and saturated by RF pulses that are targeted at slices outside the slice of interest. The MMP then interacts with the observable water, causing attenuation of its signal.[25,26] Another somewhat complementary effect is the direct attenuation of the water pool associated either with water that does not fully recover between consecutive TRs or with partial excitation of neighboring slices because of imperfect slice profile. Remarkably, these effects are also classified as MT, although they involve direct saturation of the water rather than one that is mediated by the MMP. As such, these effects are considered separately, and denoted as direct-MT (MT_{DIR}).

Previous studies have investigated the effects of incidental MT on the assessment of transverse relaxometry and biased T_2 weighting, mainly in multi-slice imaging schemes or by applying off-resonance RF pulse to saturate the MMP.[27] Uddin et al.[28] investigated the effect of reduced echo train lengths (ETL) in multi-slice MESE scans, showing the stability of fast T_2 components in the brain when shortening the ETL. Weigel et al.[29] showed that for low flip angles, the contrast of 2D multi-slice TSE sequences is less affected by the number of slices and is more sensitive to T_2 weighting rather than T_1. MacKay et al.[11] discussed the advantage of combining MT and T_2 mapping for investigating the myelin and intra-/extracellular water pools and further showed that MT will bias the T_2 nature, depending on the length and amplitude of RF pulses being used.[30]

The extent of MT-driven signal attenuation in single- and in multi-slice MESE remains an open question. Moreover, it is not always clear whether MT attenuation happens uniformly, or cumulatively, along the echo train. Specifically, a uniform attenuation will decrease the overall signal (and SNR), albeit leave the relative decay-pattern unaffected; cumulative attenuation, on the other hand, gradually builds up along the echo-train, thereby "accelerating" the signal decay and causing underestimation of the measured T_2 value.

Here, we present an analysis of MT effect on qT_2 values acquired using fast MESE protocol, and processed using the echo-modulation-curve (EMC) algorithm. This post-processing technique uses Bloch simulations of the MESE pulse-sequence to produce the true T_2 value of tissues (i.e., closely matching values obtained using single spin-echo [SSE] acquisitions).[15,16,20] EMC-based T_2 values were shown to be highly stable across protocol implementations, scanners, and scan settings, exhibiting, for example, inter-subject coefficient of variation (CV) of 2.5%, inter-scanner CV of 0.7%, and intra-scanner CV of 1.6% for in vivo brain.[31] Similar stability resulted for in vitro phantoms (unpublished) and for in vivo hip cartilage scans,[32] indicating the potential of integrating qT_2 in multi-center and longitudinal studies.[31] Herein, the effects of MT on the EMC algorithm were investigated on 3 models: an in vitro urea phantom, providing controlled settings with well-defined spectral content; an ex vivo horse brain presenting a physiological MMP content, yet free of flow or motion artifacts; and in vivo human brain. Attention was given to the different influence of MT on the acquired signal versus its influence on the ensuing T_2 values, to the difference between single-SE and multi-SE scans, and to MT dependence on MESE protocol parameters, including the echo train length, the number of slices, and the inter-slice gap.

15222594, 2019, 1, Downloaded from https://onlinelibrary.wiley.com/doi/10.1002/mrm.27704 by Tel Aviv University, Wiley Online Library on [01/02/2023]. See the Terms and Conditions (https://onlinelibrary.wiley.com/terms-and-conditions) on Wiley Online Library for rules of use; OA articles are governed by the applicable Creative Commons License

TABLE 1 MRI scan parameters

Parameter / Protocol ↓	→	TR (s)	TE (ms)	Pixel size (mm^2)	Slice thick. (mm)	BW (Hz/Px)	GRAPPA factor[60]	Inv./ref. angle	ETL	Total scan time (min) × avg
IR[a]	in vitro	13	8	1.25 × 1.25	6	200	2	180°	–	1:44 × 1
SSE	in vitro	3	10,20,…,300	1.25 × 1.25	4	200	2	180°	–	3:49 × 3
	ex vivo			0.89 × 0.89	3		1		–	9:43 × 2
MESE	in vitro	3	10	1.25 × 1.25	4	200	2	180°	30	3:49 × 3
	ex vivo	3		0.77 × 0.77	3				30	5:46 × 2
	in vivo	2.4		1.50 × 1.50	3				20	3:17 × 1

Abbreviations: BW, bandwidth; Inv., inversion; Ref., refocusing; avg, average; ETL, echo train lengths; IR, inversion recovery; MESE, multi-echo SE; SSE, single SE; thick., thickness.

[a]IR sequence used 20 TIs: (50, 125, 200, 275, 350, 390, 425, 450, 470, 500, 530, 550, 575, 600, 650, 800, 950, 1100, 1500, 2000, 5000) ms

2 | METHODS

2.1 | Samples preparation

An MRI phantom was prepared in vitro using a urea $CO(NH_2)_2$ crystal powder reagent. The urea molecule is favorable for studying the effects of MT as it contains 2 amide groups with high saturation efficiency,[33] and is free from proton-proton *J*-coupling modulations.[25,34] We note that urea MT_{SAT} is expected to be dominated by chemical exchange rather by intermolecular dipole transfer.[35,36] Six caulked 100 mL tubes were filled with distilled water and urea at concentrations of 0, 0.5, 1, 2, 3, and 4 M. The 0 M tube served as a reference solution, devoid of any MT_{SAT} effects, yet susceptible to diffusion and MT_{DIR} effects. Tubes were further doped with 0.25 mM $MnCl_2$ to reduce the water T_1/T_2 values to physiological range. The 6 tubes were inserted into a 3.3 L water container doped with 0.2 mM of $MnCl_2$. To fix the tubes' positions, 6 additional open 50 mL tubes were placed around the urea solution tubes, along with an open 100 mL tube placed at their center (Figure 1A).

A post mortem horse brain was used as a second MT model. Brain was initially fixed in formaldehyde and kept at 4°C 24 h before scanning. Then, the brain was extracted from the fixative solution, gently dried, and induced in phosphate-buffered saline (PBS) ×1 to remove residues of formaldehyde and negate the effect of aldehyde fixative with respect to the sample's T_2 and MT properties.[37] The sample was then moved to the scanner room, maintaining a constant temperature of 20°C. Immediately before the MRI scan, the brain was immersed in proton-free FC-770 Fluorinert fluid and positioned so as to fix the ventricles and cerebellum in the transverse plane (Figure 1B).

2.2 | MRI and MRS scans

All scans were performed on a whole-body 3T Siemens Prisma scanner (Siemens Healthineers, Erlangen, Germany). Comparing MT-related changes in SSE versus MESE protocols can be confounded by the fact that many MRI vendors implement SSE and MESE using 2 separate pulse sequence schemes (e.g., having different RF pulse shapes, crusher and/or spoiling gradients schemes, and parallel imaging capabilities). To circumvent this difference, we modified the MESE protocol to include single-echo mode and used it for both SSE and MESE acquisitions.

Phantom scans included MRS analysis, T_1 and T_2 measurements, and estimation of MTR. Because the intensity of MT interactions depends, among other things, on the spectral bandwidth of the MMP and its shift from water, we first assessed the spectral separation between the water and urea peak in the urea phantom using STEAM+PRESS (STRESS)

15222594, 2019, 1, Downloaded from https://onlinelibrary.wiley.com/doi/10.1002/mrm.27704 by Tel Aviv University, Wiley Online Library on [01/02/2023]. See the Terms and Conditions (https://onlinelibrary.wiley.com/terms-and-conditions) on Wiley Online Library for rules of use; OA articles are governed by the applicable Creative Commons License

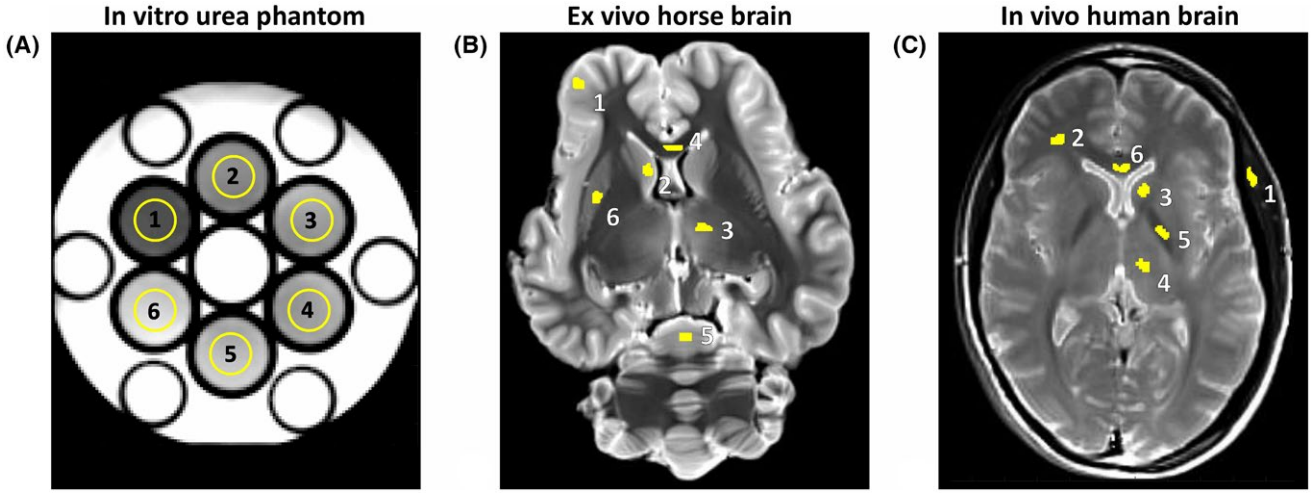

FIGURE 1 T_2-weighted images (TE = 50 ms) of the 3 models investigated in this study. (A) In vitro urea phantom, (B) ex vivo horse brain, and (C) in vivo human brain. Quantitative MTR and T_2 values were estimated for the marked ROIs, consisting of 150, 15, and 10 voxels in the urea phantom, horse brain, and human brain, respectively. ROIs in the physiological samples were marked on the T_2-weighted images as to contain as homogeneous area as possible. ROIs 1–6 in (A) correspond to urea concentrations of 0, 0.5, 1, 2, 3, and 4 M, respectively. ROIs 1–6 in (B) correspond to the cortical GM, right CN, thalamus, genu of CC, midbrain, and right putamen, respectively. ROIs 1–6 in (C) correspond to the dura matter, WM fascicles, left CN, thalamus, left GP, and genu of CC, respectively

short echo time single voxel spectroscopy (SVS).[38-40] An in-house optimized 412 ms 6-pulse water suppression scheme was played out before excitation. STRESS scan parameters were: TR/TE = 1500/15 ms; VOI = (40 mm AP) × (20 mm RL) × (15 mm IS) = 12 cc; spectral bandwidth (BW) = 2 kHz; water suppression BW = 75 Hz; vector size = 1024; T_{acq} = 512 ms; NEX = 16; $N_{dummy-scans}$ = 4. Because MESE MT_{DIR} depends on T_1 and T_1/T_2 ratio,[41-43] the T_1 values of the urea phantom were further mapped using a standard inversion recovery (IR) imaging protocol with TR > 5 × T_1 and 20 TIs (see Table 1 for a full list of scan parameters).

All in vivo data were collected for a single 30-year-old healthy male volunteer, after obtaining an informed consent and under the approval of the local Helsinki and IRB committees. Reference SSE T_2 mapping scans, free from MT, were performed on the in vitro and ex vivo models, excluding the in vivo model because of the long duration required by this scan. MT effects were evaluated on the 3 assayed models: urea phantom, ex vivo horse brain, and in vivo human brain using (1) reference (MT-free) single-slice SSE scan (excluding the in vivo model), (2) single-slice MESE, and (3) series of multi-slice MESE with increasing number of slices and with increasing inter-slice gap allowing to investigate MT dependence on scan settings. All scan parameters are delineated in Table 1.

2.3 | Data post-processing

Single voxel STRESS spectroscopic data were Fourier transformed to measure the spectral distance between the urea and water peaks. T_1 maps were generated using a standard fit of the IR images on a voxel-by-voxel basis.[44] Quantitative T_2 maps were generated using exponential fitting of the SSE data and using the EMC algorithm for the MESE data.[16] Both fitting procedures were done on a voxel-by-voxel basis after normalizing each decay curve to its first echo. We note that because of the non-exponential decay pattern of MESE protocols, the intensities of the normalized decay curves started at unity, rose in the second echo because of stimulated echo, and progressed in a fluctuating decay pattern.

TABLE 2 Urea phantom concentrations and corresponding T_1 and T_2 relaxation times

Tube no.	Urea concentration (M)	T_1 (IR) (ms)	T_2 (SSE) (ms)	T_1/T_2
1	0.0	793 ± 3	62.0 ± 0.3	12.8 ± 0.1
2	0.5	778 ± 3	60.4 ± 0.4	12.9 ± 0.1
3	1.0	763 ± 5	60.2 ± 0.3	12.7 ± 0.1
4	2.0	744 ± 2	60.1 ± 0.3	12.4 ± 0.1
5	3.0	715 ± 4	59.3 ± 0.4	12.1 ± 0.1
6	4.0	673 ± 3	58.0 ± 0.4	11.6 ± 0.1

Values denote mean ± SD, calculated for each tube within the ROIs shown in Figure 1A

15222594, 2019, 1, Downloaded from https://onlinelibrary.wiley.com/doi/10.1002/mrm.27704 by Tel Aviv University, Wiley Online Library on [01/02/2023]. See the Terms and Conditions (https://onlinelibrary.wiley.com/terms-and-conditions) on Wiley Online Library for rules of use; OA articles are governed by the applicable Creative Commons License

Following normalization, decay curves were truncated below a 0.1 threshold relative to the first echo to avoid fitting noise and the contamination from Rician noise pattern.[45] Representative T_2 maps of all 3 models can be found in the Supporting Information Figure S1.

MT-related signal attenuation was quantified by comparing the signal between single-slice SSE and single-slice MESE, and between single-slice MESE and multi-slice MESE. Although the SSE signal decays exponentially, the MESE signal is governed by stimulated echoes from the second echo and on, limiting the assessment of unbiased MTR between the 2 protocols to the first echo time only. This was calculated according to $MTR = \left(S_{\mathrm{SSE}} - S_{\mathrm{MESE}}\right) / S_{\mathrm{SSE}} \times 100\%$, where S_{SSE} denotes non-saturated magnetization from the SSE protocol, and S_{MESE} denotes the single-slice MESE signal affected by MT saturation. The second set of comparisons used single-slice MESE as a reference, and compared it to a series of multi-slice MESE scans with increasing number of slices and inter-slice gap. MTR was calculated traditionally according to[11,46]: $MTR = \left(S_{\mathrm{Single\text{ - }slice}} - S_{\mathrm{Multi\text{ - }slice}}\right) / S_{\mathrm{Single\text{ - }slice}} \times 100\%$, where $S_{\mathrm{Multi\text{ - }slice}}$ denotes the signal from the middle slice of the odd-numbered slice series, corresponding to the slice of interest, imaged in the single-slice scan. Because MTR can be measured between MESE scans separately for each echo in the series, a nominal value was calculated by averaging the MTR across the MESE echo-train. In vivo MT contrast (MTC) images were generated based on the MTR between single- and multi-slice MESE. As MTR values showed minimal variation along the echo-train, the MTR of the first-echo was used as a representative MTC value, reflecting the signal dependence on the local macromolecular content.

Mean and SD of T_1, T_2 and MTR were calculated in 6 regions-of-interest (ROIs) in the urea phantom, 6 representative ROIs in the ex vivo horse brain, and 6 representative ROIs in the human data (Figure 1). ROIs were manually segmented by a trained neuroscientist with 11 years of experience and were chosen to cover different types of tissues having a diverse range of microstructural compositions. Horse brain ROIs included the cortical gray matter (GM), right caudate nucleus (CN), thalamus, genu of corpus callosum (CC), midbrain, and right putamen. Human brain ROIs included the dura mater, white matter (WM) fascicles, left CN, thalamus, left globus pallidus (GP), and genu of CC. Aiming to factor out any tissue-related variations, small anatomic ROIs were segmented so as to minimize any heterogeneities or defragmentation of the investigated tissues.

3 | RESULTS

Table 2 presents the T_1 and T_2 values of the urea phantom calculated from single-slice IR and SSE experiments, respectively. These values were thereafter used as a reference, because these data include no saturation of the MMP and are therefore free of MT_{SAT} effect. A consistent decrease in T_1 and T_2 values was observed with increasing urea concentrations, a known effect attributed to the more restricted mobility, increased viscosity,[47] and higher dipolar coupling between water molecules in the presence of macromolecules.

The urea phantom spectrum is presented in Figure 2C exhibiting 2 peaks 128 Hz apart, one at 5.7 ppm for urea protons, and a second one at 4.7 ppm from residual water protons. To understand whether a chemical-shift related slice misregistration is expected in the presence of two proton pools, we calculated the spectral width of excited slices based on the protocol's slice-selective gradient G_{ss} and slice thickness Δz values according to: $SW_{slice} = \gamma G_{ss} \Delta z$. Given the scan settings delineated in Table 1, we found this spectral range to be 710 Hz (i.e., ±305 Hz from the slice central frequency). This indicates that the excited urea and water slices colocalize with a ~82% spatial overlap, a factor that is important for interpreting intra- and inter-slice MT interactions.

Figure 2A and B illustrate the bias in T_2 values as a result of MT when shifting from single-echo to multi-echo acquisition scheme. Similar to the finding in Table 2, a concentration-dependent reduction in T_2 is observed for both the SSE and MESE protocols, indicating the spectral broadening of the water peak in the presence of urea molecules. Although SSE is influenced by diffusion, which causes a lower apparent T_2 values (as can be seen for the MMP-free reference tube), MT produces a more dominant bias leading MESE T_2 values to be significantly lower as urea concentrations increase. Specifically, a decrease of 12.2% was measured for MESE between the reference water tube and 4 M tube versus 6.4% for SSE. The resulting dispersive graph pattern (Figure 2A) suggests that MT_{SAT} interactions bias the signal already in single-slice MESE acquisition. From spin-physics perspective, this means that MMP saturation gradually builds up along the echo train of MESE protocols, thereby "accelerating" the signal decay. Figure 2B presents the relative change in T_2 values between SSE and MESE, offering a quantitative measure of the effect size and the resulting shift from positive to negative ratio. Values exhibited a gradual decrease with increasing urea concentration, starting with a relative T_2 change of $2.0 \pm 0.8\%$ for the reference tube and decreasing down to $-4.3 \pm 1.2\%$ for the 4 M tube.

The influence of MT on the signal intensity did not systematically translate to a change in the T_2 relaxation time. Figure 3 exemplifies this by examining the correlation between T_2 and MTR. MTR values were calculated for the first echo from single slice SSE and MESE and were adjusted in this case by changing the echo train length (ETL) in the MESE scans (Figure 3A). As can be seen, the more echoes in the train, the higher is the saturation of the MESE signal because of shorter dead time between consecutive

15222594, 2019, 1, Downloaded from https://onlinelibrary.wiley.com/doi/10.1002/mrm.27704 by Tel Aviv University, Wiley Online Library on [01/02/2023]. See the Terms and Conditions (https://onlinelibrary.wiley.com/terms-and-conditions) on Wiley Online Library for rules of use; OA articles are governed by the applicable Creative Commons License

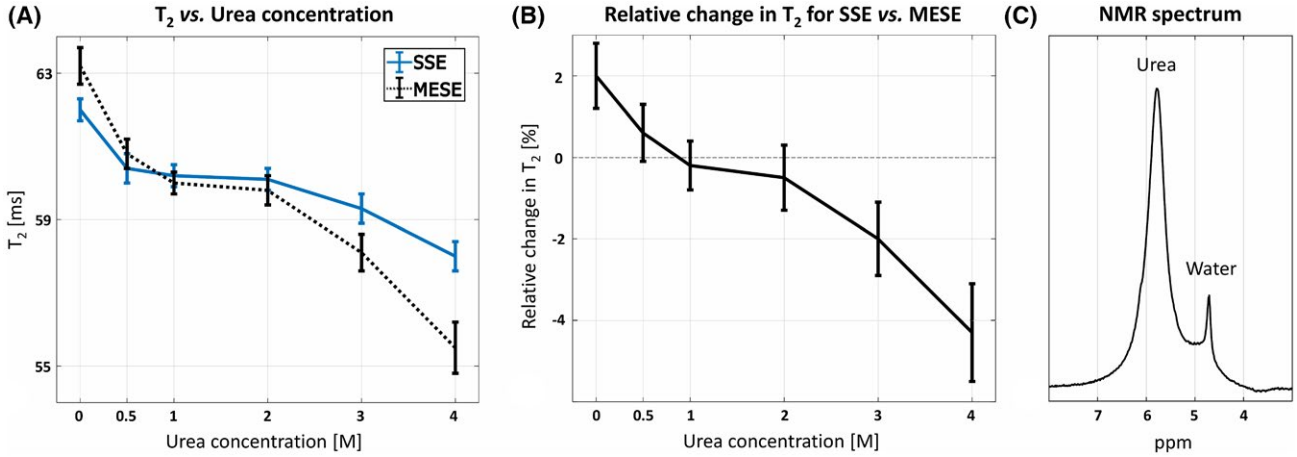

FIGURE 2 MT related urea phantom results. (A) T_2 values for SSE and MESE exhibit inverse correlation with urea concentration because of more restricted mobility and higher dipolar coupling between water molecules in the presence of macromolecules. (B) Relative change in T_2 values between MESE and SSE, calculated using $(T_{2,MESE} - T_{2,SSE})/T_{2,SSE} \times 100\%$, where $T_{2,SSE}$ considered the reference, unbiased by MT_{SAT}. Although SSE T_2 is lower at 0 M concentration because of diffusion effects, MT dominates at higher concentrations, causing MESE values to be underestimated. (C) Water suppressed single voxel spectroscopy (SVS) for the 4 M urea tube (tube 6 in Figure 1A) showing a urea peak at 5.7 ppm and a residual water peak at 4.7 ppm

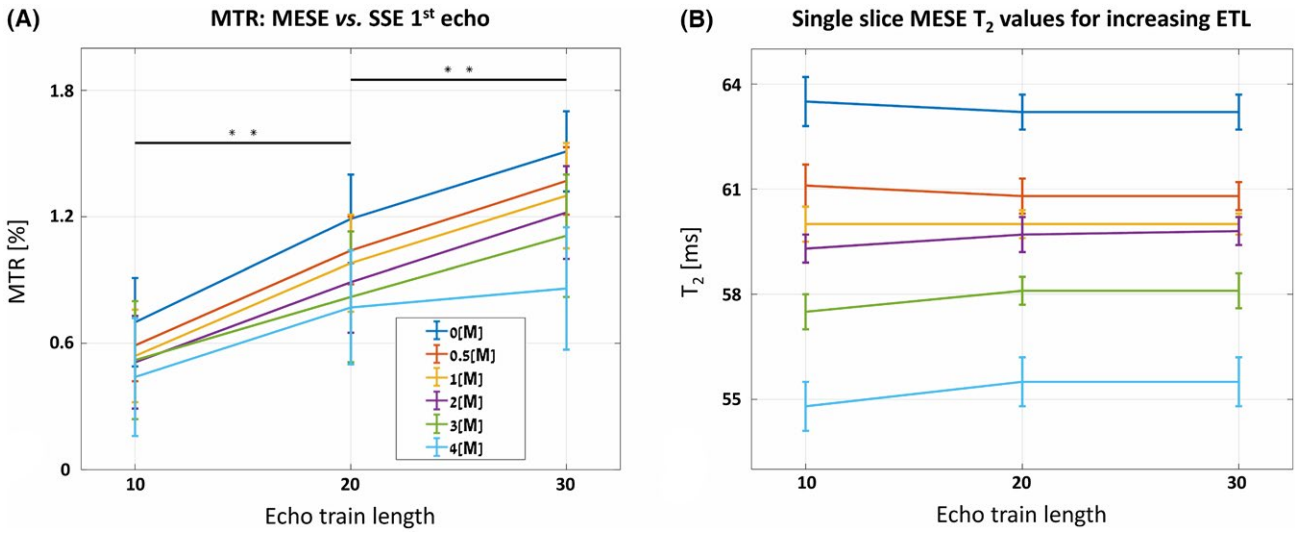

FIGURE 3 MTR and T_2 dependence on the ETL in a single-slice MESE scan of the urea phantom. (A) MTR between the 1st echo of SSE and MESE increases with longer ETLs (**$P < 0.0001$). (B) T_2 values remain stable for increasing ETLs, indicating that uniform MT attenuation occurs across the entire MESE echo train. Error bars represent SD within the ROI marked in Figure 1A

TRs. Unpaired two-tailed *t*-test of the difference in MTR for increasing ETLs was statistically significant ($P < 0.001$), with mean MTR values of 0.55 ± 0.09%, 0.95 ± 0.15%, and 1.23 ± 0.23% for ETL of 10, 20, and 30, respectively. In contrast to the signal attenuation, the matching T_2 values remained relatively constant across different ETL values, implying that MT attenuation and MTR values remained constant across the echo train.

A more endogenous representation of MT effects in MESE protocols was provided by the ex vivo horse brain having a higher macromolecular content and wider spectral width. Figure 4 presents the single slice MESE T_2 values for the 6 ROIs shown in Figure 1B, exhibiting consistent underestimation of T_2 in comparison to SSE values. Groups differences, estimated using unpaired two-tailed *t*-test, were statistically significant ($P < 0.001$) across all ROIs. MESE T_2 values were underestimated versus SSE by: cortical GM, 13.8 ± 4.7%; right CN, 5.8 ± 2.2%; thalamus, 10.4 ± 2.5%; genu of CC, 9.3 ± 7.1%; midbrain, 7.4 ± 1.4%; and putamen, 6.6 ± 1.8%. The average T_2 underestimation for all 6 ROIs was 8.9 ± 2.9%, although in the absence of non-MT reference it is impossible to isolate the contribution of MT from other factors such

15222594, 2019, 1, Downloaded from https://onlinelibrary.wiley.com/doi/10.1002/mrm.27704 by Tel Aviv University, Wiley Online Library on [01/02/2023]. See the Terms and Conditions (https://onlinelibrary.wiley.com/terms-and-conditions) on Wiley Online Library for rules of use; OA articles are governed by the applicable Creative Commons License

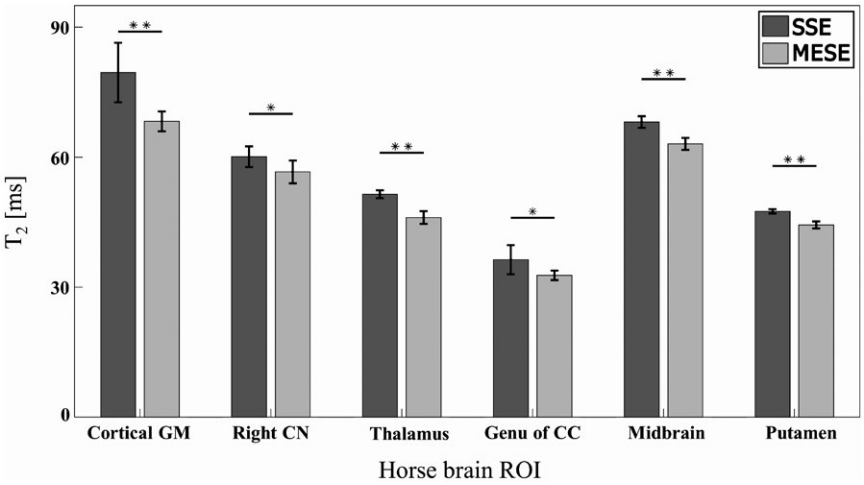

FIGURE 4 Underestimation of T_2 values in a single-slice MESE scan of the ex vivo horse brain. T_2 values were estimated within 6 representative ROIs for single-slice SSE and MESE protocols, showing consistent MT-related underestimation of MESE derived values. $*P < 0.001$; $**P < 0.0001$. Cohen's d effect size was found to be very large ($d > 1.2$) in the (*) ROIs and huge ($d > 2.0$) in the (**) ROIs

as diffusion. The Cohen d criterion that measures the effect size was also calculated to estimate the mean T_2 differences between MESE and SSE values. According to Cohen et al.,[48] the criterion is defined by $d = (\overline{T_{2,\mathrm{SSE}}} - \overline{T_{2,\mathrm{MESE}}})/(\text{pooled SD})$, where $\overline{T_{2,x}}$ represent the mean spatial T_2 value from protocol x. This yielded a standardized effect-size of "huge" ($d > 2.0$) in the cortical GM, thalamus, midbrain, and putamen and "very large" ($d > 1.2$) in the LCN and genu of CC.[49]

The shift from single to multi-slice acquisitions is traditionally viewed as a major cause of MT bias. This is exemplified in Figure 5, presenting the MTC in a human brain between single- and multi-slice scans and for different number of slices and inter-slice gaps. An increased signal loss is exhibited in the MTC maps for increased number of slices, generating an image contrast, which correlated with the tissues' macromolecular content. A reversed effect appeared for increased inter-slice gap, as both MT_{DIR} from overlapping slice profiles and MT_{SAT} from off-resonance saturation are decreased. Numeric single-slice versus multi-slice MTR and T_2 values are shown in Figure 6 for the 3 assayed models and for different number of slices and inter-slice gaps. MTR correlated positively with the number of slices, with smallest increase observed in the urea phantom because of its lower macromolecular content in relation to the physiological tissues. The mean MTR values in Figure 6 were averaged across all ROIs in each model, displaying a non-linear growth of total 2.8% in vitro, 18.5% ex vivo, and 18.9% in vivo when increasing the number of slices. We note that the in vivo brain and in vitro urea, phantom MTR compared 3 and 9 slices with zero inter-slice gap, whereas ex vivo horse brain MTR compared 3 and 7 slices with 50% gap, causing the ex vivo MTR to have a relatively lower MTR baseline. However, its similarity to the average in vivo MTR change suggests that both brain models share similar MMPs.

In contrast to the elevation in MTR, a negligible and inconsistent change was observed in the corresponding T_2 values (Figure 6D–F). This T_2 stability once again implies that, for all 3 models, a constant MT attenuation occurs across all echoes in the train. The level of MTR is, in turn, determined by the amount of MT_{DIR} and by the extent of off-resonance saturation of the MMP in the slice-of-interest when scanning other slices in the series. It is important to note that the intra-slice MT_{SAT} (i.e., saturation that develops across the echo train) does not contribute to the single-versus-multi slice MTR, because it occurs similarly in any MESE scan regardless of the number of acquired slices.

Figure 7 shows the dependence of MTR and T_2 on the inter-slice gap in multi-slice MESE scans. As can be seen in Figure 7A–C, increasing the gap lowers off-resonance saturation, thereby reducing the corresponding MTR levels. The MTR attenuation for the ex vivo and in vivo tissues (Figure 7B and C) was moderate and, in most cases, consistent. Contrary to that, the in vitro urea model (Figure 7A) exhibited a sharp drop in the MTR for high inter-slice gap, owing to the narrow spectral range of the MMP in this phantom and the high localization of the urea and water slices (see Figure 2C). All corresponding T_2 values (Figure 7D–F) exhibited no correlation with the inter-slice gap, suggesting that, akin to when increasing number of slices, any signal attenuation occurs similarly across the entire echo train. MTR reduction when shifting from 0% to 200% gap was averaged across all ROIs, displaying a non-linear decline of 21.6%, 11.5%, and 21.2% for the in vitro (9 slices), ex vivo (7 slices), and in vivo (9 slices) models, respectively. Note that for the in vitro phantom, a small MTR of $3.3 \pm 0.2\%$ was measured at 200% gap, most probably as a result of partial longitudinal recovery of the water molecules in the slice of interest.

To gain more insight into the baseline macromolecular content of each model, normalization was applied to the MTR values in Figure 7A–C, with respect to the case of 0% inter-slice gap. This normalization allowed to factor out the dependence on scan setting and isolate the effect of increasing gap values in relation to the spectral range of the

15222594, 2019, 1, Downloaded from https://onlinelibrary.wiley.com/doi/10.1002/mrm.27704 by Tel Aviv University, Wiley Online Library on [01/02/2023]. See the Terms and Conditions (https://onlinelibrary.wiley.com/terms-and-conditions) on Wiley Online Library for rules of use; OA articles are governed by the applicable Creative Commons License

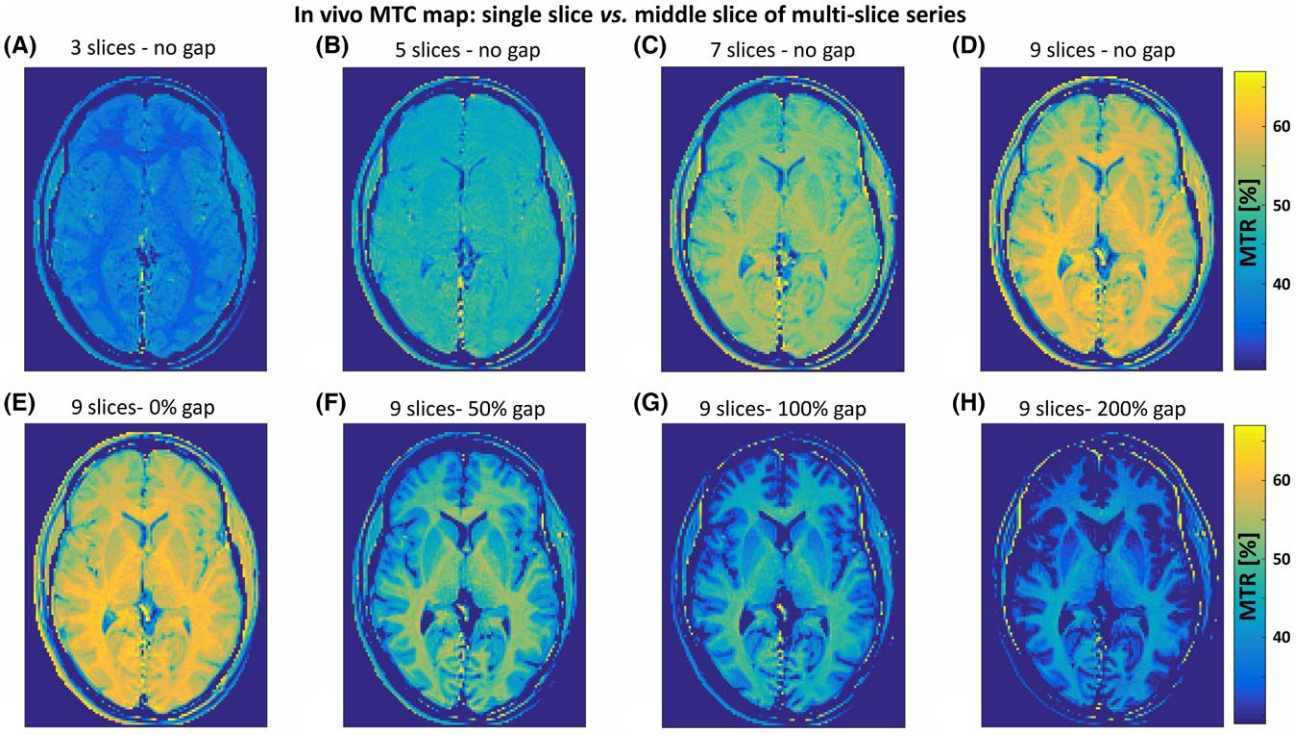

FIGURE 5 In vivo human brain MTC maps. MT contrast is based on the 1st echo MTR between a single-slice and the middle slice of multi-slice scan series. (A–D) MTC for increasing number of slices (gap 0%). (E–H) MTC for increasing inter-slice gap for a 9-slice series

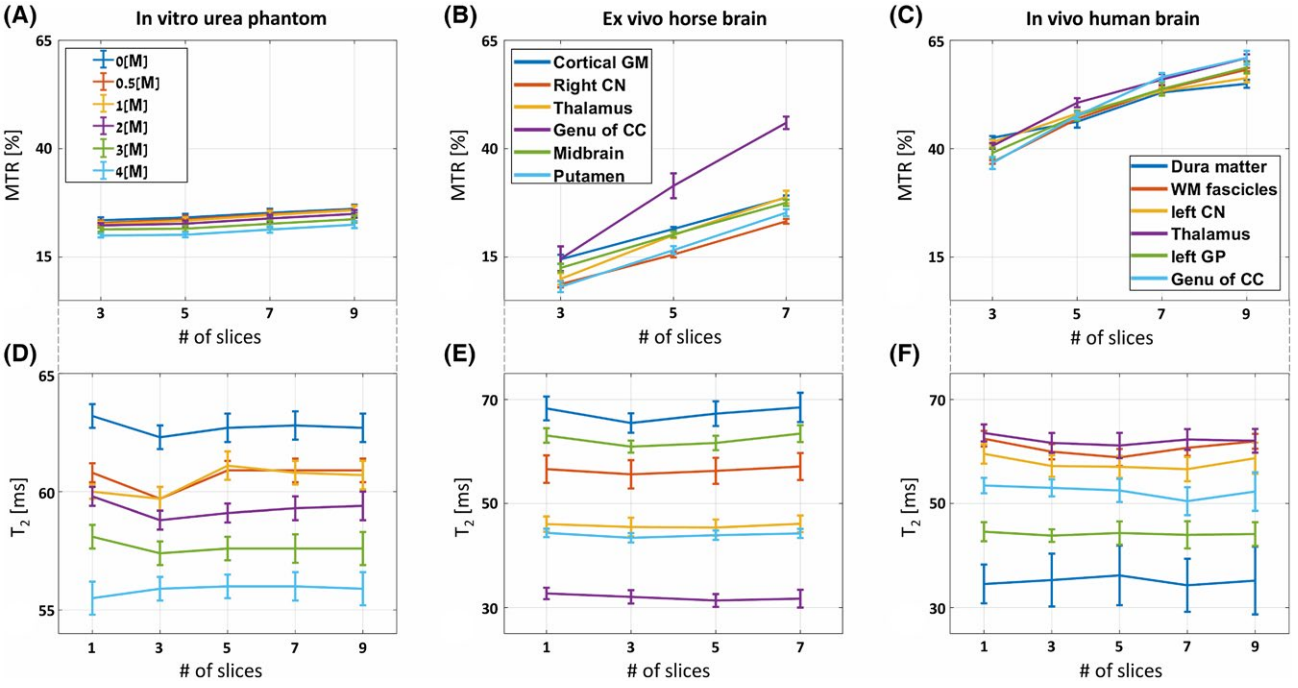

FIGURE 6 Multi-slice MESE MTR (A–C) and T_2 values (D–F) as a function of increasing number of slices. Values are presented for all 3 models investigated in this study: (A and D) in vitro urea phantom; (B and E) ex vivo horse brain; and (C and F) in vivo human brain. MTR was measured between single-slice acquisition and the middle slice in a multi-slice scan series. MTR exhibits positive correlation with the number of slices and with the higher amount of macromolecules characterizing the physiological tissues. No trend was seen in the corresponding T_2 values (D–F), suggesting that MT attenuation was constant across the MESE echo train. We note the relatively low MTR baseline in the ex vivo scans (B) because of the fact these scans used a 50% inter-slice gap versus a 0% gap in the other models (A and C)

15222594, 2019, 1, Downloaded from https://onlinelibrary.wiley.com/doi/10.1002/mrm.27704 by Tel Aviv University, Wiley Online Library on [01/02/2023]. See the Terms and Conditions (https://onlinelibrary.wiley.com/terms-and-conditions) on Wiley Online Library for rules of use; OA articles are governed by the applicable Creative Commons License

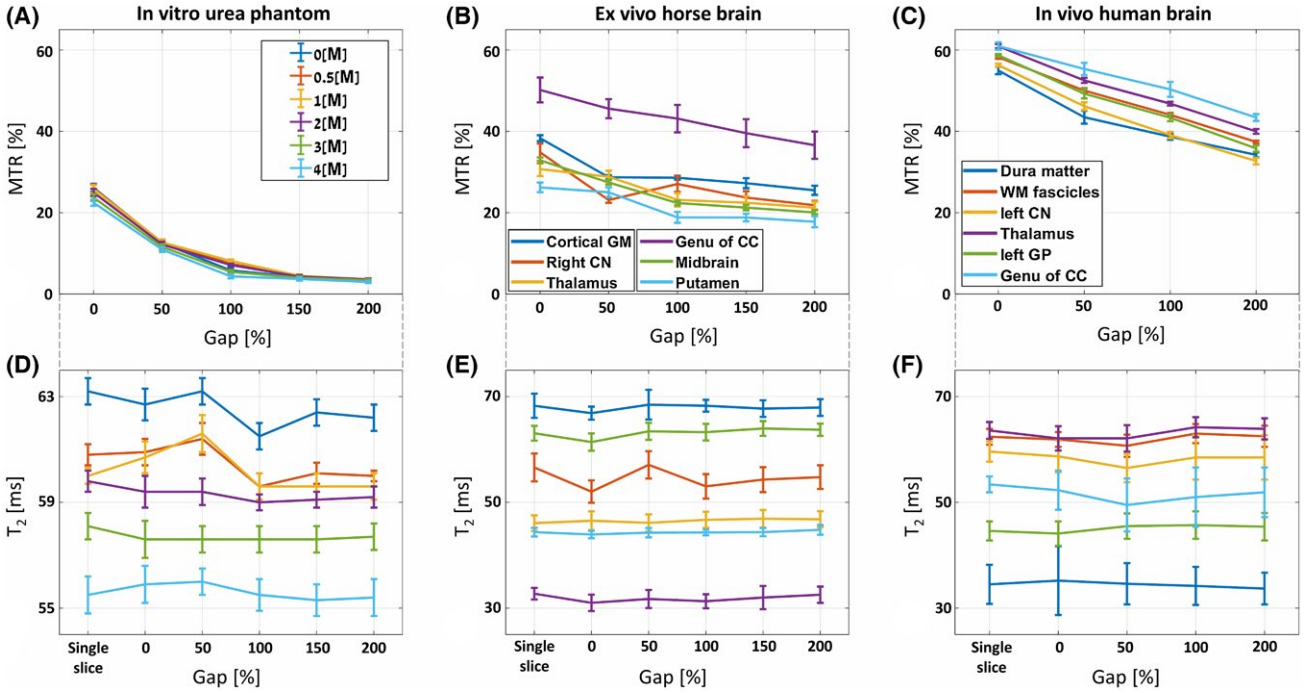

FIGURE 7 Multi-slice MESE MTR (A–C) and T_2 values (D–F) as a function of increasing inter-slice gap. Values are presented for all 3 models investigated in this study: (A and D) in vitro urea phantom; (B and E) ex vivo horse brain; and (C and F) in vivo human brain. MTR was calculated between single-slice acquisition and the middle slice in a multi-slice scan series ($N_{slices} = 7$ for ex vivo [B and E] and 9 for in vitro [A and D] and in vivo [C and F]). MTR exhibited inverse correlation with the inter-slice gap, and positive correlation with the higher macromolecular content characterizing the physiological tissues. No trend, however, was found in the corresponding T_2 values, suggesting that MT levels are constant across the MESE echo train

MMP. Results from all ROIs were averaged together, normalized, and are presented in Figure 8. Two very clear patterns emerge from this figure: first, the highly similar macromolecular content of the two physiological tissues (horse brain and human brain), and second, their strong disparity from the synthesized urea solution. Whereas the urea phantom exhibits a relatively low macromolecular content, the physiological tissues, although from completely different sources, produce higher MTR with very similar dependence on inter-slice gap, suggesting a similar spectral distribution of their MMPs.

4 | DISCUSSION

4.1 | Saturation of the MMP in MESE protocols leads to underestimation of T_2

The results presented in this article demonstrate that MT can bias MESE-based quantification of T_2 values in vivo. The extensive use of high power RF pulses in this acquisition scheme saturates the macromolecules residing in physiological samples, which, in turn, exchange their magnetization with the mobile water molecules through chemical-exchange and magnetization-transfer interactions. These two mechanisms cannot be distinguished from one another and are conjointly labeled as $MT_{SAT.}$[50] Both interactions, however, involve incidental saturation of the MMP, leading to attenuation of the water signal, and in certain settings, to underestimation of the measured T_2 relaxation times. A third type of signal attenuation, linked to the extensive use of RF pulses, is the direct saturation of the water pool due to slice-profile interactions or incomplete T_1 recovery between TRs. Also categorized as MT, this latter mechanism is separately denoted as MT_{DIR} and was found to cause a uniform attenuation of all echoes in the train, thereby having little influence on the normalized signal decay curve and the ensuing T_2 values. From a practical point of view, multi-slice acquisitions are designed to alleviate MT_{DIR} effects related to slice-profile imperfections by interleaving the slice order. This means that instead of acquiring slices sequentially (i.e., ascending or descending order), the series of odd-numbered slices are acquired first and then the even-numbered slices.[17,25,26,51-53]

Quantifying the effects of MT during an in vivo scan is highly challenging because of extensive scan-times associated with the need to acquire both MESE and a reference SSE data. The urea molecules, which appear endogenously in the body (e.g., in the urine, kidneys, and blood),[54] provided a good model for studying MT at controlled levels, having a well-defined and measurable spectral content. The urea peak is located 1 ppm away from water, translating to ~128 Hz at 3T. Because of the relatively large slice bandwidth used

15222594, 2019, 1, Downloaded from https://onlinelibrary.wiley.com/doi/10.1002/mrm.27704 by Tel Aviv University, Wiley Online Library on [01/02/2023]. See the Terms and Conditions (https://onlinelibrary.wiley.com/terms-and-conditions) on Wiley Online Library for rules of use; OA articles are governed by the applicable Creative Commons License

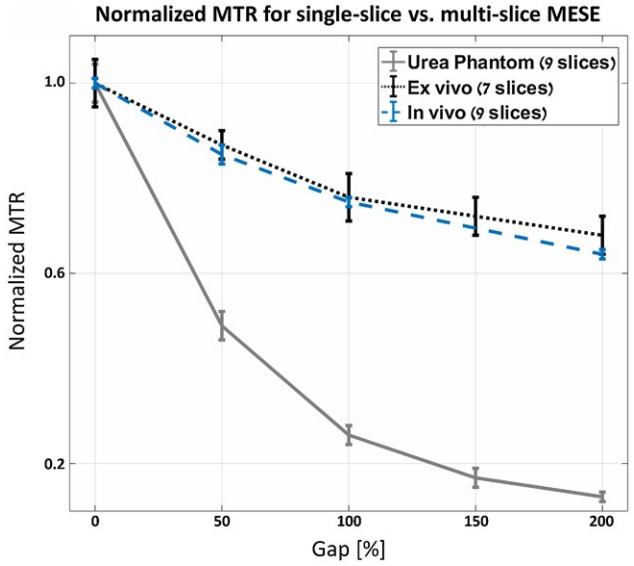

FIGURE 8 Normalized MTR values calculated for the data shown in Figure 7A–C and averaged across all ROIs. Normalization allowed us to eliminate differences relating to scan settings and isolate the MMP effect on MTR, highlighting the similarity between the two physiological tissues, as opposed to their discrepancy from the urea phantom model

in most imaging experiments, this spectral difference meant that the urea–water slice misregistration is much smaller than the slice thickness, leading MT_{SAT} effects to emerge already in single slice acquisitions as was seen in Figure 2A and B. Specifically, the presence of urea molecules had a 2-fold influence on the water signal. First, a decrease in baseline T_2 was observed, attributed to increased dipole-dipole interactions with the 2 hydrophilic amide groups. The soluble urea molecules slow the diffusion and rapid rotation of the smaller water molecules leading to longer intermolecular coherence time and corresponding faster relaxation.[55] The second effect of urea was MT with the water, further attenuating the signal and accelerating its relaxation rate. Although the intrinsic decrease in T_2 baseline occurs already in SSE, this protocol is not affected by MT, but rather susceptible to a secondary diffusion-related attenuation because of its use of very long echo times. Juxtaposing SSE's diffusion effect vis-à-vis the MT attenuation of MESE signals, we found the latter to be more dominant (see Figure 2), causing higher attenuation of the signal and ultimately leading to underestimation of MESE T_2 values. The higher MT saturation efficiency of amide protons in the urea molecules accentuated the MT effects in this model.[33] Although endogenous molecules are characterized by a typically lower exchange rate (e.g., mean residence time of 100s of ms for myelin)[56] and lower corresponding saturation efficiency, the overall MT effects in the in vivo models did not differ significantly from the urea phantom. We attribute this to the larger spectral range and higher fraction of the MMP in vivo. MTR was therefore analyzed similarly in all models, reflecting the overall transfer of magnetization occurring within MESE protocol timescales.

The RF train in MESE schemes constitutes the driving force for intra-slice MT_{SAT}, accelerating the signal attenuation, and eventually translating into underestimation of T_2. The RF shape, duration, and amplitude will significantly affect the acquired signal by governing the pattern of both stimulated echoes and MT.[18] Identifying this dependence on the RF pulse properties, we compared SSE and MESE qT_2 values using a modified MESE scheme that can act as a single SE experiment, thereby factoring out any implementation differences and, more importantly, by using the EMC technique that factors out the signal contamination by stimulated echoes that otherwise mask MT effects.

4.2 | Accumulated versus uniform saturation of MESE echo train

One of the key findings of our study was that MT-related bias of T_2 is caused by pure MT_{SAT}, occurring already within the confines of a single-slice MESE echo-train. As more RF pulses are applied along the train, intra-slice MMP saturation accumulates and the signal attenuation increases. This accelerates the MESE signal decay and manifests as shorter T_2 value as can be seen in the SSE versus MESE dispersion pattern in Figure 2B.

Direct water saturation (i.e., MT_{DIR}) also affects the signal in a single-slice acquisitions, albeit, by uniformly decreasing the steady-state magnetization across the entire decay curve. In this case, MT_{DIR} from on-resonance water saturation will decrease the initial available magnetization in any given TR because of partial T_1 recovery, as the TR is significantly smaller than $5\times T_1$. This is supported by the stability of the T_2 values for different ETLs, in contrast to the respective increase in MTR (Figure 3). The average SSE versus MESE MTR for ETL=10, 20, and 30 was found to be $0.55 \pm 0.09\%$, $0.95 \pm 0.15\%$, and $1.23 \pm 0.23\%$, respectively, implying that the signal does not undergo full longitudinal recovery between consecutive TRs, thereby lowering the equilibrium magnetization when using longer ETLs.

The accumulated signal attenuation caused by MT_{SAT}, on the other hand, had a similar effect on all train lengths, leading to very similar T_2 values. Increasing the ETL from 10 to 20 or 30 had a minor effect on ensuing T_2 values, because the MMP is already highly saturated at the 10th echo for physiological T_2 components. Therefore, the additional saturation at later echoes, where the signal has already decayed, will not cause significant change of the decay pattern.

Interestingly, the MTR in the increasing ETL experiment inversely correlated with urea concentrations, presenting higher MTR for the reference water tube, and lower MTR for the 4 M tube. This behavior resulted from the fact that the amount of MT_{DIR} experienced by the slice of interest is

15222594, 2019, 1, Downloaded from https://onlinelibrary.wiley.com/doi/10.1002/mrm.27704 by Tel Aviv University, Wiley Online Library on [01/02/2023]. See the Terms and Conditions (https://onlinelibrary.wiley.com/terms-and-conditions) on Wiley Online Library for rules of use; OA articles are governed by the applicable Creative Commons License

ultimately governed by the T_1/T_2 ratio and by the absolute T_1 value.[42,43] In our case, the presence of urea affected T_1 more than T_2 (see Table 2) leading to lower MT_{DIR} at higher concentration. These findings were further corroborated by the fact that MTR indeed diminished to zero when using $TR > 5 \times T_1$ (result not shown), confirming the hypothesis that the MT effects in Figure 3A consist chiefly from water-related MT_{DIR} between consecutive TRs.

4.3 | Multi-slice acquisitions attenuate the signal baseline but do not alter the corresponding T_2 values

Traditionally, MT bias is associated with explicit MT preparation or with multi-slice acquisition schemes, where the MMP in the slice-of-interest is being saturated while acquiring neighboring slices. This is generally valid when considering the MT influence on the signal amplitude and will reflect in T_2-weighted images.[26,57] MT_{sat}-related signal attenuation in multi-slice acquisitions occurs separately in each TR and in two modes, where only one of them biases the measured T_2. One mode develops by the on-resonance RF pulses applied during the excitation and refocusing of the investigated slice, and the second mode results from off-resonance RF pulses applied during the acquisition of other slices. The first on-resonance mode will affect the MR signal gradually as the MT_{SAT} develops along the RF train, decreasing the measured signal, and translating into underestimation of T_2. The second off-resonance mode, on the other hand, will not bias the measured T_2, but only decrease the initial transverse magnetization in the slice of interest. This will not change the decay pattern, therefore leaving the T_2 values unaffected.

An increase in saturation, and a corresponding elevation in MTR, was observed when shifting from single- to multi-slice acquisitions. This was well correlated with the spectral characteristics of the macromolecules in the phantom and in the representative ROIs that were chosen within the ex vivo and in vivo brains. Owing to their broad MMP spectral content, a more significant multi-slice effect was observed in the physiological tissues. As expected, positive correlation was observed with increased number of slices because of the larger number of RF pulses applied. Negative correlation was observed with increased inter-slice gap, first, because of the fact that less MT_{SAT} from excitation of other slices occurs in the slice-of-interest as the spectral distance between the slices increases, and second, because of reduced slice cross-talk. This was mostly apparent in the urea phantom having a limited spectral width, and causing MTR to drop almost to zero for high inter-slice gap (Figure 7A). Both the slice crosstalk (MT_{DIR}) and off-resonance saturation (MT_{SAT}) is largely circumvented in multi-slice scans by employing the interleaved slice ordering scheme.[17] This reduces the direct saturation from excitation of adjacent slices and partly alleviates off resonance excitation of the MMP in the slice of interest. The MT-related signal variations for different number of slices or inter-slice gap did not translate to a change in the measured T_2 values, because all echoes in the MESE train were attenuated in a uniform manner, resulting in a similar decay pattern. As illustrated in Figures 6 and 7, this finding was stable across all models used in this study.

We note that the ex vivo experiment was executed before the in vivo scans, whereas some of the parameters were optimized when running the subsequent in vivo experiments. One example is the ETL, which was reduced to 20 in the in vivo scans, because this ETL was found to be sufficient for producing stable T_2 value (see "signal truncation" in the EMC method, under data post-processing). From SAR perspective, shortening the echo-train allowed to increase the number of slices to 9 in vivo versus 7 slices ex vivo. This parameter difference did not change the final conclusion, because both the number of slices and the inter-slice gap did not change the measured T_2 values.

4.4 | Tissue composition and compartmentation

Apart from scan parameters and macromolecular composition, MT interactions, and the corresponding bias in T_2, are also directly influenced by tissue microarchitecture. This results from the existence of several sub-voxel compartments or from partial voluming effects at tissue edges. By using homogeneous and well-defined ROIs, rather the whole brain structures, we avoided the latter effect, while minimizing variations because of different tissue compartmentations.

As can be seen in Figure 8, the physiological samples had similar MT characteristics, with small variability occurring between different types of tissues. One frequently investigated example is white matter compartmentalization into extra-cellular water, intra-cellular water, and water trapped between myelin sheaths. As suggested by MacKay et al.,[43] the short and long T_2 components in this type of tissue might respond differently to MT effects, with the overall T_2 bias being dependent on the local relative fraction of the two. Another example is the coexistence of water and fat molecules within the same voxel causing a complex signal bias (e.g., fat in the muscle or hematopoietic bone marrow).[58,59] These tissues present another level of complication, as each sub-compartment can have different T_1 and T_2 relaxation times and therefore experience a different MT bias. As part of our ongoing work, we are investigating the estimation of quantitative T_2 and MT in multi-T_2 environments, aiming to characterize, and subsequently correct for, MT bias in specific tissue types and within different brain structures.

15222594, 2019, 1, Downloaded from https://onlinelibrary.wiley.com/doi/10.1002/mrm.27704 by Tel Aviv University, Wiley Online Library on [01/02/2023]. See the Terms and Conditions (https://onlinelibrary.wiley.com/terms-and-conditions) on Wiley Online Library for rules of use; OA articles are governed by the applicable Creative Commons License

5 | CONCLUSIONS

MT interactions have a non-negligible influence on in vivo MESE acquisitions. This manifests either as a uniform attenuation of the entire echo train, which leaves the T_2 values unaffected, or as a cumulative decrease of the signal, which translates to an underestimation of T_2 values. Our results revealed an overall MT-related T_2 bias in the range of −4.3–2.0% in vitro, and 5.8–13.8% ex vivo. Between the two mechanisms classified as MT, the cumulative, intra echo-train saturation of the MMP (i.e., MT_{SAT}) was found to affect T_2, whereas direct water saturation (i.e., MT_{DIR}) had an impact on the signal amplitude. From a practical point of view, however, it is the integrated effect of protocol settings, the macromolecular spectral-content, and tissue compartmentation that will determine the final amount of MT_{SAT} and MT_{DIR}, and whether they bias the measured T_2 values.

In the current study, we adopted the EMC algorithm as a T_2 mapping technique. This was crucial factor for disentangling the influence of stimulated echoes and MT interactions, allowing genuine analysis of the effects of MT in MESE protocols. We believe that the ensuing results can be generalized to any type of T_2 postprocessing technique, as long as it correctly incorporates the influence of stimulated echoes and B_1^+ inhomogeneities. Improving the overall understanding of MT mechanisms in MESE protocols will facilitate the development of new acquisition or postprocessing schemes that will eventually negate or compensate for these effects (e.g., Ehses et al.[23]) and yield more accurate quantification of relaxation times. Expanding the EMC simulations to model 2- or 3-pools is highly challenging from computational point of view and is part of ongoing work. Such models are, moreover, tissue-specific as they depend on the microscopic architecture of the tissue being investigated. Our multi-slice results (Figures 6 and 7) provide some optimism as they imply that multi-slice EMC simulations are not necessarily required for modeling MT when quantifying the T_2 relaxation value, as most of the accumulated signal attenuation occurs within the confines of the echo train and the slice of interest.

ORCID

Noam Ben-Eliezer https://orcid.org/0000-0003-2944-6412

REFERENCES

1. Siemonsen S, Mouridsen K, Holst B, et al. Quantitative T2 values predict time from symptom onset in acute stroke patients. *Stroke*. 2009;40:1612–1616.
2. Lund H, Jønsson A, Andresen J, Rostrup E, Paulson OB, Sørensen PS. Cognitive deficits in multiple sclerosis: correlations with T2 changes in normal appearing brain tissue. *Acta Neurol Scand*. 2012;125:338–344.
3. Drayer B, Burger P, Darwin R, Riederer S, Herfkens R, Johnson GA. MRI of brain iron. *AJR Am J Roentgenol*. 1986;147:103–110.
4. Floris S, Blezer EL a, Schreibelt G, et al. Blood-brain barrier permeability and monocyte infiltration in experimental allergic encephalomyelitis: a quantitative MRI study. *Brain*. 2004;127(Pt3):616–627.
5. Eitel I, Friedrich MG. T2-weighted cardiovascular magnetic resonance in acute cardiac disease. *J Cardiovasc Magn Reson*. 2011;13:13.
6. Liu W, Turkbey B, Senegas J, et al. Accelerated T2 mapping for characterization of prostate cancer. *Magn Reson Med*. 2011;65:1400–1406.
7. Pan J, Pialat JB, Joseph T, et al. Knee cartilage T2 characteristics and evolution in relation to morphologic abnormalities detected at 3-T MR imaging: a longitudinal study of the normal control cohort from the osteoarthritis initiative. *Radiology*. 2011;261:507–515.
8. Poon CS, Henkelman RM. Practical T2 quantitation for clinical applications. *J Magn Reson Imaging*. 1992;2:541–553.
9. Deoni SCL. Transverse relaxation time (T2) mapping in the brain with off-resonance correction using phase-cycled steady-state free precession imaging. *J Magn Reson Imaging*. 2009;30:411–417.
10. Sled JG, Pike GB. Correction for B1 and B0 variations in quantitative T2 measurements using MRI. *Magn Reson Med*. 2000;43:589–593.
11. MacKay A, Laule C, Vavasour I, Bjarnason T, Kolind S, Mädler B. Insights into brain microstructure from the T2 distribution. *Magn Reson Imaging*. 2006;24:515–525.
12. Hennig J. Multiecho imaging sequences with low refocusing flip angles. *J Magn Reson*. 1988;78:397–407.
13. Lebel RM, Wilman AH. Transverse relaxometry with stimulated echo compensation. *Magn Reson Med*. 2010;64:1005–1014.
14. Prasloski T, Mädler B, Xiang QS, MacKay A, Jones C. Applications of stimulated echo correction to multicomponent T2 analysis. *Magn Reson Med*. 2012;67:1803–1814.
15. McPhee KC, Wilman AH. Transverse relaxation and flip angle mapping: evaluation of simultaneous and independent methods using multiple spin echoes. *Magn Reson Med*. 2017;77:2057–2065.
16. Ben-Eliezer N, Sodickson DK, Block TK. Rapid and accurate T2 mapping from multi spin echo data using Bloch-simulation-based reconstruction. *Magn Reson Med*. 2015;73:809–817.
17. Constable RT, Anderson AW, Zhong J, Gore JC. Factors influencing contrast in fast spin-echo MR imaging. *Magn Reson Imaging*. 1992;10:497–511.
18. Deoni SCL, Peters TM, Rutt BK. High-resolution T1 and T2 mapping of the brain in a clinically acceptable time with DESPOT1 and DESPOT2. *Magn Reson Med*. 2005;53:237–241.
19. Blystad I, Warntjes JBM, Smedby O, Landtblom AM, Lundberg P, Larsson EM. Synthetic MRI of the brain in a clinical setting. *Acta Radiol*. 2012;53:1158–1163.
20. Ben-Eliezer N, Sodickson DK, Shepherd T, Wiggins GC, Block KT. Accelerated and motion-robust in vivo T2 mapping from radially undersampled data using Bloch-simulation-based iterative reconstruction. *Magn Reson Med*. 2016;75:1346–1354.
21. Ma D, Gulani V, Seiberlich N, et al. Magnetic resonance fingerprinting. *Nature*. 2013;495:187–192.
22. Majumdar S, Orphanoudakis SC, Gmitro A, O'Donnell M, Gore JC. Errors in the measurements of T2 using multiple-echo MRI techniques I. Effects of radiofrequency pulse imperfections. *Magn Reson Med*. 1986;3:397–417.

15222594, 2019, 1, Downloaded from https://onlinelibrary.wiley.com/doi/10.1002/mrm.27704 by Tel Aviv University, Wiley Online Library on [01/02/2023]. See the Terms and Conditions (https://onlinelibrary.wiley.com/terms-and-conditions) on Wiley Online Library for rules of use; OA articles are governed by the applicable Creative Commons License

23. Ehses P, Seiberlich N, Ma D, et al. IR TrueFISP with a golden-ratio-based radial readout: fast quantification of T1, T2, and proton density. *Magn Reson Med*. 2013;69:71–81.
24. Zhang J, Kolind SH, Laule C, MacKay AL. How does magnetization transfer influence mcDESPOT results? *Magn Reson Med*. 2015;74:1327–1335.
25. Santyr GE. Magnetization transfer effects in multislice MR imaging. *Magn Reson Imaging*. 1993;11:521–532.
26. Dixon WT, Engels H, Castillo M, Sardashti M. Incidental magnetization transfer contrast in standard multislice imaging. *Magn Reson Imaging*. 1990;8:417–422.
27. Harrison R, Bronskill MJ, Mark Henkelman R. Magnetization transfer and T2 relaxation components in tissue. *Magn Reson Med*. 1995;33:490–496.
28. Uddin MN, Marc Lebel R, Wilman AH. Transverse relaxometry with reduced echo train lengths via stimulated echo compensation. *Magn Reson Med*. 2013;70:1340–1346.
29. Weigel M, Helms G, Hennig J. Investigation and modeling of magnetization transfer effects in two-dimensional multislice turbo spin echo sequences with low constant or variable flip angles at 3 T. *Magn Reson Med*. 2010;63:230–234.
30. Deoni SCL, Rutt BK, Peters TM. Rapid combined T1 and T2 mapping using gradient recalled acquisition in the steady state. *Magn Reson Med*. 2003;49:515–526.
31. Shepherd TM, Kirov II, Charlson E, et al. New rapid, accurate T2 quantification detects pathology in normal-appearing brain regions of relapsing-remitting MS patients. *Neuroimage Clin*. 2017;14:363–370.
32. Ben-Eliezer N, Yoshimoto AE, Block KT, et al. A new method for accurate detection of cartilage lesions in femoroacetabular impingement using quantitative T2 mapping : preliminary validation against arthroscopic findings at 3 T. In Proceedings of the 24th Annual Meeting of ISMRM, Singapore, 2016. Abstract 2272.
33. Van Zijl PCM, Yadav NN. Chemical exchange saturation transfer (CEST): what is in a name and what isn't? *Magn Reson Med*. 2011;65:927–948.
34. Bruce Pike G, Glover GH, Hu BS, Enzmann DR. Pulsed magnetization transfer spin-echo MR imaging. *J Magn Reson Imaging*. 1993;3:531–539.
35. Dagher AP, Aletras A, Choyke P, Balaban RS. Imaging of urea using chemical exchange-dependent saturation transfer at 1.5 T. *J Magn Reson Imaging*. 2000;12:745–748.
36. Liepinsh E, Otting G. Specificity of urea binding to proteins. *J Am Chem Soc*. 1994;116:9670–9674.
37. Shepherd TM, Thelwall PE, Stanisz GJ, Blackband SJ. Aldehyde fixative solutions alter the water relaxation and diffusion properties of nervous tissue. *Magn Reson Med*. 2009;62:26–34.
38. Volovyk O, Tal A. Application of phase rotation to STRESS localization scheme at 3 T. *Magn Reson Med*. 2018;79:2481–2490.
39. Bottomley PA, inventor; General Electric Company, assignee. *Selective volume method for performing localized NMR spectroscopy*. US Patent 4,480,228. October 30, 1984.
40. Tal A, Gonen O. Spectroscopic localization by simultaneous acquisition of the double-spin and stimulated echoes. *Magn Reson Med*. 2015;73:31–43.
41. Moran PR, Hamilton CA. Near-resonance spin-lock contrast. *Magn Reson Imaging*. 1995;13:937–946.
42. Ulmer JL, Mathews VP, Hamilton CA, Elster AD, Moran PR. Magnetization transfer or spin-lock? An investigation of off-resonance saturation pulse imaging with varying frequency offsets. *AJNR Am J Neuroradiol*. 1996;17:805–819.
43. Vavasour IM, Whittall KP, Li DK, MacKay AL. Different magnetization transfer effects exhibited by the short and long T2 components in human brain. *Magn Reson Med*. 2000;44:860–866.
44. Kaldoudi E, Williams SCR. Relaxation time measurements in NMR imaging. Part I: longitudinal relaxation time. *Concepts Magn Reson*. 1993;5:217–242.
45. Gudbjartsson H, Patz S. The Rician distribution of noisy MRI data. *Magn Reson Med*. 1995;34:910–914.
46. Henkelman RM, Stanisz GJ, Graham SJ. Magnetization transfer in MRI: a review. *NMR Biomed*. 2001;14:57–64.
47. Kawahara K, Tanford C. Viscosity and density of aqueous solutions of urea and guanidine hydrochloride. *J Biol Chem*. 1966;241:3228–3232.
48. Cohen J. *Statistical power analysis for the behavioral sciences*, 2nd Edition. New York: Routledge; 2013:567.
49. Sawilowsky S. New effect size rules of thumb. *J Mod Appl Stat Methods*. 2009;8:597–599.
50. van Zijl PCM, Lam WW, Xu J, Knutsson L, Stanisz GJ. Magnetization transfer contrast and chemical exchange saturation transfer MRI. Features and analysis of the field-dependent saturation spectrum. *NeuroImage*. 2018;168:222–241.
51. McPhee KC, Wilman AH. T1 and T2 quantification from standard turbo spin echo images. *Magn Reson Med*. 2019;81:2052–2063.
52. Majumdar S, Orphanoudakis SC, Gmitro A, O'Donnell M, Gore JC. Errors in the measurements of T2 using multiple-echo MRI techniques. II. Effects of static field inhomogeneity. *Magn Reson Med*. 1986;3:562–574.
53. Crawley AP, Henkelman RM. Errors in T2 estimation using multislice multiple-echo imaging. *Magn Reson Med*. 1987;4:34–47.
54. Liu L, Mo H, Wei S, Raftery D. Quantitative analysis of urea in human urine and serum by 1H nuclear magnetic resonance. *Analyst*. 2012;137:595–600.
55. Edzes HT, Samulski ET. The measurement of cross-relaxation effects in the proton NMR spin-lattice relaxation of water in biological systems: hydrated collagen and muscle. *J Magn Reson*. 1978;31:207–229.
56. Dortch RD, Harkins KD, Juttukonda MR, Gore JC, Does MD. Characterizing inter-compartmental water exchange in myelinated tissue using relaxation exchange spectroscopy. *Magn Reson Med*. 2013;70:1450–1459.
57. Kucharczyk W, Crawley AP, Kelly WM, Henkelman RM. Effect of multislice interference on image contrast in T2- and T1-weighted MR images. *AJNR Am J Neuroradiol*. 1988;9:443–451.
58. Machann J, Stefan N, Schick F. 1H MR spectroscopy of skeletal muscle, liver and bone marrow. *Eur J Radiol*. 2008;67:275–284.
59. Marty B, Baudin PY, Reyngoudt H, et al. Simultaneous muscle water T2 and fat fraction mapping using transverse relaxometry with stimulated echo compensation. *NMR Biomed*. 2016;29:431–443.
60. Griswold MA, Jakob PM, Heidemann RM, et al. Generalized autocalibrating partially parallel acquisitions (GRAPPA). *Magn Reson Med*. 2002;47:1202–1210.

SUPPORTING INFORMATION

Additional supporting information may be found online in the Supporting Information section at the end of the article.

15222594, 2019, 1, Downloaded from https://onlinelibrary.wiley.com/doi/10.1002/mrm.27704 by Tel Aviv University, Wiley Online Library on [01/02/2023]. See the Terms and Conditions (https://onlinelibrary.wiley.com/terms-and-conditions) on Wiley Online Library for rules of use; OA articles are governed by the applicable Creative Commons License

FIGURE S1 Representative T_2 maps of in vitro urea phantom (A and B), ex vivo horse brain (C and D), and in vivo human brain (E and F). SSE, single spin echo; MESE, multi echo spin echo (ETL 20 or 30). Maps are shown for different scan settings: single slice (A–C and E); multi slice with N_{slices} 5 and 50 inter slice gap (D); and multi slice with N_{slices} 9 and 100 inter slice gap (F)

How to cite this article: Radunsky D, Blumenfeld-Katzir T, Volovyk O, et al. Analysis of magnetization transfer (MT) influence on quantitative mapping of T_2 relaxation time. *Magn Reson Med*. 2019;82:145–158. https://doi.org/10.1002/mrm.27704

15222594, 2019, 1, Downloaded from https://onlinelibrary.wiley.com/doi/10.1002/mrm.27704 by Tel Aviv University, Wiley Online Library on [01/02/2023]. See the Terms and Conditions (https://onlinelibrary.wiley.com/terms-and-conditions) on Wiley Online Library for rules of use; OA articles are governed by the applicable Creative Commons License